ARTICLE

Synthesis, structures, and reactivity of isomers of [RuCp*(1,4-(Me$_2$N)$_2$C$_6$H$_4$)]$_2$†

Received 00th January 20xx,
Accepted 00th January 20xx

DOI: 10.1039/x0xx00000x

Elena Longhi,[a] Chad Risko,[b] John Bacsa,[c] Victor Khrustalev,[d,e] Sergei Rigin,[d] Karttikay Moudgil,[a] Tatiana V. Timofeeva,[d] Seth R. Marder[a,f,g,h,i] and Stephen Barlow*[,a,f]

[RuCp*(1,3,5-R$_3$C$_6$H$_3$)]$_2$ {Cp* = η^5-pentamethylcyclopentadienyl, R = Me, Et} have previously been found to be moderately air stable, yet highly reducing, with estimated D$^+$/0.5D$_2$ (where D$_2$ and D$^+$ represent the dimer and the corresponding monomeric cation, respectively) redox potentials of ca. –2.0 V vs. FeCp$_2^{+/0}$. These properties have led to their use as n-dopants for organic semiconductors. Use of arenes substituted with π–electron donors is anticipated to lead to even more strongly reducing dimers. [RuCp*(1-(Me$_2$N)-3,5-Me$_2$C$_6$H$_3$)]$^+$PF$_6^-$ and [RuCp*(1,4-(Me$_2$N)$_2$C$_6$H$_4$)]$^+$PF$_6^-$ have been synthesized and electrochemically and crystallographically characterized; both exhibit D$^+$/D potentials slightly more cathodic than [RuCp*(1,3,5-R$_3$C$_6$H$_3$)]$^+$. Reduction of [RuCp*(1,4-(Me$_2$N)$_2$C$_6$H$_4$)]$^+$PF$_6^-$ using silica-supported sodium-potassium alloy leads to a mixture of isomers of [RuCp*(1,4-(Me$_2$N)$_2$C$_6$H$_4$)]$_2$, two of which have been crystallographically characterized. One of these isomers has a similar molecular structure to [RuCp*(1,3,5-Et$_3$C$_6$H$_3$)]$_2$; the central C—C bond is *exo*,*exo*, *i.e.*, on the opposite face of both six-membered rings from the metals. A D$^+$/0.5D$_2$ potential of –2.4 V is estimated for this *exo*,*exo* dimer, more reducing than that of [RuCp*(1,3,5-R$_3$C$_6$H$_3$)]$_2$ (–2.0 V). This isomer reacts much more rapidly with both air and electron acceptors due to a much more cathodic D$_2^+$/D$_2$ potential than those of [RuCp*(1,3,5-R$_3$C$_6$H$_3$)]$_2$. The other isomer to be crystallographically characterized, along with a third isomer, are both dimerized in an *exo*,*endo* fashion, representing the first examples of such dimers. Density functional theory calculations and reactivity studies indicate that the central bonds of these two isomers are weaker than those of the *exo*,*exo* isomer, or of [RuCp*(1,3,5-R$_3$C$_6$H$_3$)]$_2$, leading to estimated D$^+$/0.5D$_2$ potentials of –2.5 and –2.6 V vs. FeCp$_2^{+/0}$. At the same time the D$_2^+$/D$_2$ potentials for the *exo*,*endo* dimers are anodically shifted relative to those of [RuCp*(1,3,5-R$_3$C$_6$H$_3$)]$_2$, resulting in much greater air stability than for the *exo*,*exo* isomer.

Introduction

Reduction of [RuCp*(η^6-arene)]$^+$ salts {Cp* = η^5-pentamethylcyclopentadienyl} – either electrochemically or by alkali-metal reductants – can lead to formation of dimers, [RuCp*(arene)]$_2$, in which the hapticity of the arene ligand is reduced to η^5 and an arene-arene bond is formed, as shown for the case of [RuCp*(1,3,5-R$_3$C$_6$H$_3$)]$^+$ (R = Me, Et), **1**$^+$ and **2**$^+$, in Scheme 1.[1-3] The dimers **1$_2$** and **2$_2$** are powerful reductants with effective reducing potentials, E(D$^+$/0.5D$_2$) where D$^+$ and D$_2$ denote monomeric cation and dimer, respectively, of ca. –2.0 V vs. FeCp$_2^{+/0}$,[4] yet are, due to the coupling of redox and bond-cleavage processes, sufficiently inert that they can be briefly handled in air.[3] These properties, coupled with their solution and vacuum processibility, make these dimers versatile n-dopants for increasing conductivity and/or facilitating electron injection in a wide range of organic semiconductors,[3,5-10] including, if photoactivated, molecules with reduction potentials as negative as ca. –2.2 V,[11] and for modifying the properties of electrode surfaces and of low-dimensional materials.[12-18] Related dimeric n-dopants with similar properties have been obtained through reduction of [FeCp*(C$_6$H$_6$)]$^+$,[3,4] rhodocenium and iridocenium ions,[3-5,12,19-22] and 2-substituted 1,3-dimethylbenzo[*d*]imidazolium cations.[10,23-26]

The effective reducing potential is given by:

$$E(D^+/0.5D_2) = E(D^+/D) + \Delta G_{diss}/2F \qquad (1)$$

where E(D$^+$/D) is the reducing potential of the neutral 19-electron monomer, ΔG_{diss} is the free energy of dissociation of the neutral dimer, and F is the Faraday constant.[4] This equation clearly indicates that stronger dopants may be obtainable by

[a] *School of Chemistry and Biochemistry & Center for Organic Photonics and Electronics, Georgia Institute of Technology, Atlanta, GA 30332-0400, USA.*
[b] *Department of Chemistry & Center for Applied Energy Research (CAER), University of Kentucky, 125 Chemistry-Physics Building, Lexington, KY 40506, USA.*
[c] *Crystallography Lab, Emory University, 201 Dowman Drive, Atlanta, GA 30322, USA.*
[d] *Department of Chemistry, New Mexico Highlands University, Las Vegas, NM 87701, USA.*
[e] *Department of Inorganic Chemistry, Peoples' Friendship University of Russia, Moscow 117198, Russia.*
[f] *Renewable and Sustainable Energy Institute (RASEI), University of Colorado Boulder, Boulder, CO 80303, USA. E-mail: stephen.barlow@colorado.edu*
[g] *Department of Chemical and Biological Engineering , University of Colorado Boulder, Boulder, CO 80303, USA.*
[h] *Department of Chemistry, University of Colorado Boulder, Boulder, CO 80303, USA.*
[i] *Chemistry and Nanoscience Center, National Renewable Energy Laboratory, Golden, CO 80401, USA.*

† Electronic Supplementary Information (ESI) available: Crystallographic data, NMR spectra, voltammograms, vis.-NIR spectra, and other additional discussion and figures. CCDC-2079705, 2080755, 2083852, and 2083960. For ESI and crystallographic data in CIF or other electronic format see DOI: 10.1039/x0xx00000x

dimerizing more reducing monomers and/or by weakening the central C—C bonds of dimers, for example, through steric strain, although there is often a partial cancelation of these effects: for example, the IrCp*Cp monomer is much more reducing than its Rh analogue, but the bond in the corresponding dimer is also considerably stronger.[4] Moreover, as seen when comparing $[RhCp^*Cp]_2$ and $[RhCp^*Cp'']_2$ (Cp'' = C_5Me_4H), the use of methylation to cathodically shift $E(D^+/0.5D_2)$ via $E(D^+/D)$ can also result in more cathodic values of $E(D_2^{\bullet+}/0.5D_2)$ and consequently increased air sensitivity.[4] Another possible means of obtaining a more reducing monomer may be to incorporate π-electron donors such as amino groups into the monomers. Here we report the synthesis, structures, and reactivity of the reduction products of $[RuCp^*(\eta^6\text{-}1,4\text{-}(Me_2N)_2C_6H_4)]^+$, along with density functional theory (DFT) calculations that give insight into the properties of these compounds.

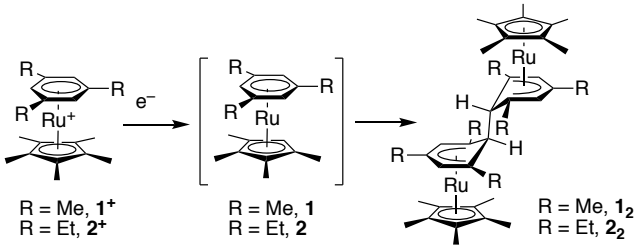

Scheme 1. Reduction of 18-electron RuCp*(arene) cations to 19-electron monomers, followed by dimerization to regain an 18-electron configuration around each metal center.

Results and discussion

Synthesis and structures of [RuCp*(arene)]+ salts

We synthesized hexafluorophosphate salts of $[RuCp^*(\eta^6\text{-arene})]^+$ cations **3**+ (arene = 1-(Me_2N)-3,5-$Me_2C_6H_3$) and **4**+ (arene = 1,4-$(Me_2N)C_6H_4$) by the standard procedure[27] of heating the arene with $[RuCp^*(NCMe)_3]^+PF_6^-$ in refluxing 1,2-dichloroethane (Scheme 2).**Scheme 2.** Synthesis of NMe_2-substituted $[RuCp^*(\eta^6\text{-arene})]$+ salts and reductive dimerization of **4**+ (DCE = 1,2-dichloroethane, NaK_2-SG(I) = silica-gel supported Na:K alloy).

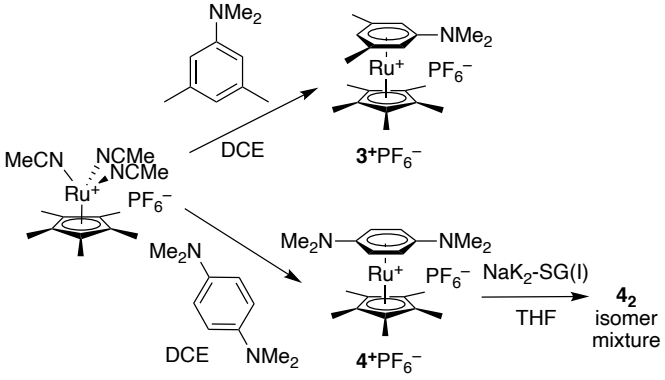

Scheme 2. Synthesis of NMe_2-substituted $[RuCp^*(\eta^6\text{-arene})]^+$ salts and reductive dimerization of **4**+ (DCE = 1,2-dichloroethane, NaK_2-SG(I) = silica-gel supported Na:K alloy).

Single-crystal X-ray structures were determined for both **3**+$[PF_6]^-$ and **4**+$[PF_6]^-$. Their molecular structures (Fig. 1) are broadly similar to those of other $[RuCp^*(arene)]^+$ salts,[28-31] including those of **1**+I^- and **2**+PF_6^- (see Table S1, †ESI).[1032] However, in **3**+, as in other RuCp*arene complexes with π-donor arene substituents, such as $[RuCp^*(C_6H_5NMe_2)]^+BF_4^-$ (**I**+BF_4^-)[33] $RuCp^*(C_6H_5O)\bullet 2PhOH$ (**II**•2PhOH),[34] and $RuCp^*(2,6\text{-}^tBu_2\text{-}C_6H_3O)$ (**III**),[35] the arene is somewhat folded such that the π-donor-substituted carbon is more distant from the metal, consistent with distortion towards an η^5-cyclohexadienyl ligand with an exo-iminium or keto group (Scheme 3; see also section S1 of the †ESI for more a detailed discussion). In **4**+ both amino-substituted carbons are folded away from the metal.

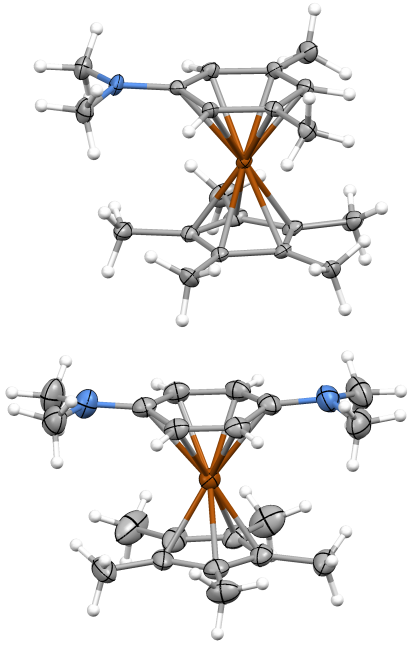

Fig. 1. Molecular structures of **3**+ (above) and **4**+ (below) from X-ray structures of their $[PF_6]^-$ salts (50% thermal ellipsoids).

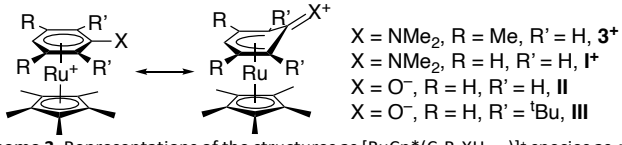

Scheme 3. Representations of the structures as $[RuCp^*(C_6R_nXH_{5-n})]^+$ species as η^6-arene and η^5-cyclohexadienyl complexes, along with chemical structures of some examples of such species included in Table 2.

Reduction of [RuCp*(arene)]+ salts

$E(D^+/D)$ values were measured using cyclic voltammetry in THF / 0.1 M $Bu_4N^+PF_6^-$ (Figs S2-3, †ESI). Consistent with what is seen for many other $[RuCp^*(\eta^6\text{-arene})]^+$ derivatives,[1,2,4,32,36] the corresponding oxidation waves are ill-defined and the corresponding peak oxidations currents, I_{ox}, seen are much lower than the reduction currents, I_{red}, implying rapid dimerization or other chemical reactions occur following formation of the 19-electron compound. Furthermore, as in many of those other cases, subsequent to scanning the irreversible reduction of the cations, irreversible oxidation peaks are seen. In the case of **4**+, this peak is seen at ca. –0.9 V vs. $FeCp_2^{+/0}$, which is close to the potentials at which $\mathbf{1_2}$ and $\mathbf{2_2}$ are oxidized,[4] suggesting that a dimer may be formed. Indeed, as discussed below, two of the isomers of $\mathbf{4_2}$ are oxidized at very similar potentials (Fig. S2, †ESI). On the other hand, the

electrochemical reduction product of $\mathbf{3}^+$ is oxidized at ca. +0.3 V vs. $FeCp_2^{+/0}$ (Fig. S3, †ESI), a potential much more oxidizing than expected for a dimer and likely even for a DH derivative (ruthenium pentamethylcyclopentadienyl 1,3,5-trimethylcyclohexa-1,3-dien-5-yl, the hydride-reduction product of $\mathbf{1}^+$, is irreversibly oxidized at ca. –0.3 V[37]).

While NMe_2 is a powerful π-donor in organic chemistry, it has a less dramatic effect in metal-sandwich compounds, where the relevant frontier orbitals have large metal contributions. Thus, the 17/18-electron $[FeCp(C_5H_4NMe_2)]^{+/0}$ and $[Fe(C_5H_4NMe_2)_2]^{+/0}$ redox couples are seen at –0.36 and –0.63 V vs. $FeCp_2^{+/0}$,[38] and, of more relevance here, the 18/19-electron $[Co(C_5H_4NMe_2)_2]^{+/0}$ couple is at a potential 0.37 V more reducing than that of $[CoCp_2]^{+/0}$.[39] The $E(D^+/D)$ potentials shown in Table 1 for $[RuCp^*(\eta^6\text{-arene})]^+$ cations also indicate only moderate effects of the NMe_2 substituents. The $\mathbf{3}^+/\mathbf{3}$ and $\mathbf{4}^+/\mathbf{4}$ potentials are similar, with the two alkyl substituents of the first apparently having more-or-less the same effect as the NMe_2 group of the latter. The reduction potentials for the two new cations are a little more cathodic than those for $\mathbf{1}^+$ and $\mathbf{2}^+$, but not quite as cathodic as that for $RuCp^*(1,3,5\text{-}(Me_3SiCH_2)_3C_6H_3]^+$ (–2.96 V).[32]

Table 1. Electrochemical Potentials (V vs. $FeCp_2^{+/0}$ in THF / 0.1 M Bu_4NPF_6) for RuCp*(arene) Cations and Dimers.

D	$E_{red}(D^+/D)$	$E_{ox}(D_2^+/D_2)$
1 [a]	–2.67	–1.10
2 [a]	–2.70	–1.09
3	–2.91	*b*
4	–2.89	–1.41 (**4₂a**), –0.88 (**4₂b**)
5 [c]	–2.71	*b*

[a] Data from ref. 4. [b] Dimer not isolated. [c] See Scheme 4 below and Fig. S3, †ESI.

Chemical reductions were carried out in THF using sodium amalgam (Na:Hg), sodium-potassium alloy (Na:K), and stage I silica-gel-supported sodium-potassium alloy (NaK_2-SG(I)),[40] a commercially available reductant that is considerably less hazardous than unsupported Na:Hg or Na:K, being stable in dry air, and that has recently been shown to be effective in the synthesis of $\mathbf{1}_2$.[10] Reduction of both $\mathbf{3}^+$ and $\mathbf{4}^+$ afford material with complex NMR spectra suggesting mixtures of products. However, it proved possible to separate and characterize the reduction products of $\mathbf{4}^+$, as discussed in the following section.

The formation of product mixtures is not particularly surprising since many $[Ru(\eta^5\text{-}C_5R_nH_{5-n})(\eta^6\text{-arene})]^+$ cations fail to cleanly dimerize on reduction: hydride-reduced species,[1] products originating from ligand exchange,[1] and two-electron reduction[32] have all been reported; we have also observed deprotonation of $[RuCp^*(1,3,5\text{-}^tBu_3C_6H_3)]$, $\mathbf{5}^+$, to form a η^4-1,2,3,4-tetramethylfulvene complex, **6** (Scheme 4, see section S3 and Fig. S4 of †ESI). Moreover, some 19-electron compounds that cleanly dimerize, notably $RuCp(1,3,5\text{-}Me_3C_6H_3)$ and $IrCp^*Cp$,[1,41] do so to form mixtures of regioisomers. Moreover, trends in reactivity are not always straightforward: for example, although Na:Hg reduction of $[RuCp^*(1,3,5\text{-}Me_3C_6H_3)]^+$ results in clean dimerization, its C_6H_6 and C_6Me_6 analogues form $RuCp^*(\eta^5\text{-areneH})$ species under the same conditions.[1]

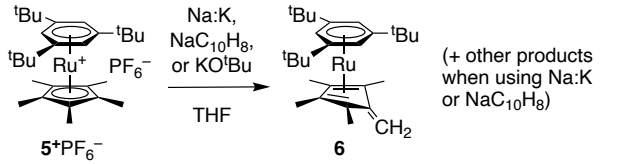

$\mathbf{5}^+PF_6^-$ **6**

Scheme 4. Deprotonation of a [RuCp*(arene)]+ to form a fulvene complex.

Separation and characterization of $[RuCp^*(1,4\text{-}(Me_2N)C_6H_4)]_2$ isomers

One component of the mixture formed on reduction of $\mathbf{4}^+$ by NaK_2-SG(I) was more poorly soluble in diethyl ether than the others and so could be isolated cleanly by removal of the other isomers by brief extraction with this solvent. This more poorly soluble fraction, $\mathbf{4_2a}$, was found to be unusually air sensitive compared to $\mathbf{1_2a}$ and $\mathbf{2_2a}$. If one assumes that **4** dimerizes through the arene and that in both sandwich units the central C–C bond is on the opposite face of the ligand from the metal (*exo,exo*) – as in all sandwich-compound dimers structurally characterized to date – four regio- and diastereoisomers are possible; these are shown in Scheme 5 along with their highest possible symmetries (note that the second and third are chiral so will exist as pairs of enantiomers). NMR spectra (Fig. S5 and S8, †ESI) of $\mathbf{4_2a}$, which show a single Cp* CH_3 resonance, two NMe_2 resonances, and four CH resonances, are consistent with formation of either the C_i- or C_2-symmetric CH–CH bonded isomers. X-ray crystallography (see below) indicates it is the C_i isomer.

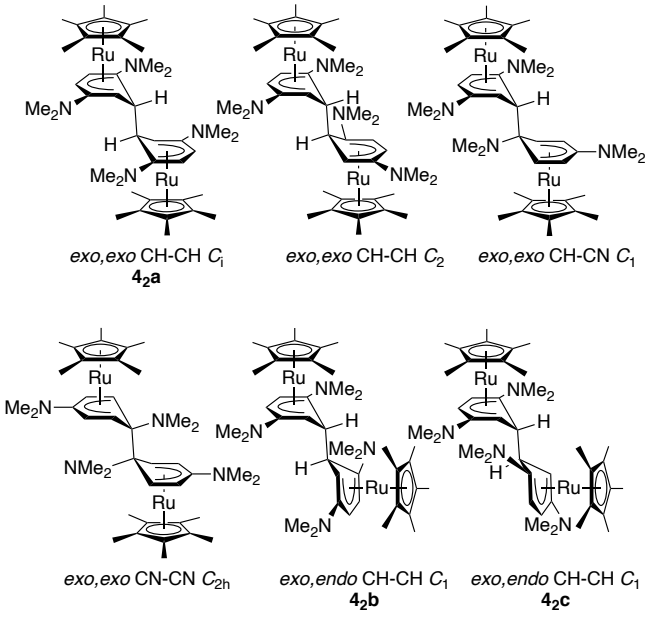

Scheme 5. Some isomers of $[RuCp^*(1,4\text{-}(Me_2N)C_6H_4)]_2$, $\mathbf{4_2}$, including all four possible exo,exo arene-arene isomers, one which ($\mathbf{4_2a}$) is isolated, and two of the possible exo,endo isomers ($\mathbf{4_2b}$-**c**), which are also isolated. All six of these are considered computationally (see Table 3). The highest symmetry point group that can be adopted by each isomer is indicated.

The ether extracts were found to contain some additional $\mathbf{4_2a}$, which, taking advantage of its air sensitivity, could be removed by brief exposure to air and washing with acetonitrile. The remaining mixture contained a major ($\mathbf{4_2b}$) and minor species ($\mathbf{4_2c}$), which could not easily be separated. However, both $\mathbf{4_2b}$ and $\mathbf{4_2c}$ were obtained substantially NMR-pure in small

quantities, and their ^{1}H and ^{13}C NMR spectra (see Figs. S6-7, S9-10, †ESI) were assigned using a variety of 1D and 2D techniques. Both **4₂b** and **4₂c** are clearly low-symmetry species, each having two inequivalent Cp* groups, four inequivalent NMe_2 groups, and eight CH resonances. The coupling patterns and 2D COSY spectra indicate that both dimers are CH–CH linked, but that, in contrast to **4₂a** (or the other possible *exo,exo* CH-CH isomer shown in Scheme 5) the two monomer units are inequivalent. A single-crystal X-ray determination for **4₂b** (see following section) indicates that the inequivalence arises because, while for one monomer unit the central C—C bond is on the opposite face of the arene from metal (*exo*), as is the case for **4₂a** and all other sandwich-compound dimers structurally characterized to date, the C—C bond is, unprecedently, on the same face as the metal (*endo*) in the other monomer unit.

4₂c exhibits qualitatively similar NMR spectra to **4₂b** and acccordingly is assigned the other possible CH—CH-linked *exo,endo* isomer (Scheme 5). Further details of the NMR spectra of **4₂b** and **4₂c** are discussed in more detail in section S4 of the †ESI.

Crystal structures of [RuCp*(1,4-(Me₂N)₂C₆H₄)] isomers

As noted above, the crystal structures of **4₂a** and **4₂b** were determined. That of **4₂a** (Fig. 2) confirms that, like **1₂** and **2₂**, this molecule is dimerized through CH positions of each arene ring and that the central C—C bridge is *exo,exo*, i.e. on the opposite faces of the arene ligands from the metals. The molecule has crystallographic C_i symmetry in the crystal, and so exhibits a perfectly staggered conformation about the central C–C bond, characterized by a centroid–C_{ipso}–C'$_{ipso}$-centroid' torsion angle, ϕ (Fig. 3), of 180°. This is similar to the conformation adopted by **2₂**, which has crystallographic C_{2h} symmetry.[4] Detailed structural parameters (see Fig. 3 for definitions) are compared with those of **2₂** in Table 2.

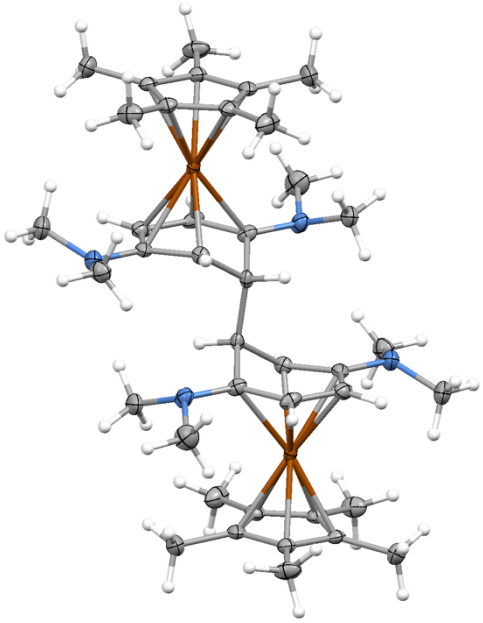

Fig. 2. Molecular structure of **4₂a** (50% thermal ellipsoids) determined by X-ray crystallography.

Table 2. Selected Crystallographic Parameters (Å, °) for $[RuCp^*(arene)]_2$ Species.

Dimer	ϕ [a]	$r(C_{ipso}–C'_{ipso})$ [b]	r(Ru–C$_{arene}$) [c]	r(Ru–C_{ipso}) [d]	α [e]	β [f]
2₂ [g]	180	1.559(2)	2.161(1)–2.246(1)	2.860	0.3	51.9
4₂a	180	1.544(4)	2.177(2)-2.325(2)	2.864	2.6	48.3
4₂b	154.0	1.562(1)	2.1658(10)-2.3312(9)[h]	2.879 [h]	4.3 [h]	49.0 [h]
			2.1607(9)-2.2540(9)[i]	2.823 [i]	9.9 [i]	43.3 [i]

[a] Cen–C_{ipso}–C'$_{ipso}$-Cen' torsion angle, where Cen and Cen' are the centroids defined by the coordinated carbon atoms of the arene ligands, and C_{ipso} and C'$_{ipso}$ are the two arene C atoms through which the compound is dimerized. [b] Central C—C bond of dimer. [c] Range of bond lengths from Ru to the η^5 bridging ligand. [d] Non-bonded distance from Ru to the C atom of the six-membered ring through which the compound is dimerized. [e] Ring tilt in the sandwich moiety: the angle between the plane defined by the coordinated Cp* C atoms and that defined by the coordinated bridging ligand C atoms. [f] Fold angle in the six-membered ring: the angle between the plane defined by the five coordinated C atoms and that defined by the bridgehead carbon and the two adjacent coordinated C atoms. [g] From ref. 4. [h,i] Denote the monomer units with *exo* and *endo* intermonomer C—C bonds respectively.

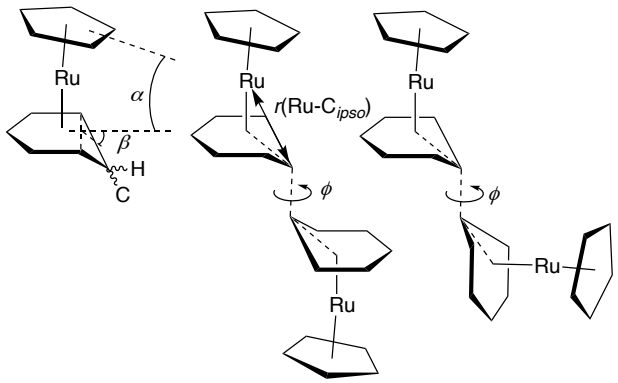

Fig. 3. Schematic representation of some of the structural parameters for π-donor-substituted $[RuCp^*(arene)]_2$ dimer structures compared in Table 2 and discussed in the text. See footnote to Table 2 for more detailed definitions.

Isomer **4₂b** (Fig. 4) is also linked through CH positions of the arene ring, but there is neither crystallographic nor approximate molecular symmetry since this an *exo,endo*-connected dimer, i.e., one in which the central C—C bond is on the opposite face from the metal in one monomer, but on the *same* face for the other. All other dimers of 19-electron sandwich complexes to have been crystallographically characterized to date – including **2₂**,[4] $[Fe(C_5R_5)(C_6H_6)]_2$ {R = H, Me},[4,42] and various rhodocene and iridocene dimers[4] – have been *exo,exo* dimers. Crystallographically determined structures of related species where "piano stool" species are dimerized through the carbocyclic ligand – $[Mn(arene)(CO)_3]_2$ derivatives,[43,44] $[Mo(^tBu_3C_7H_4)(CO)_3]_2$,[45] and the unsymmetric "dimer" formed between $Mn(C_6H_6)(CO)_3$ and $W(C_7H_7)(CO)_3$[46] – have also been *exo,exo* isomers. Even $[K(C_6H_6)$(18-crown-

6)]$_2$,[47] where the metal arene-interaction is presumably considerably less covalent and the bridging ligand characterized by a much smaller fold angle β, is *exo,exo*. Nor has the existence of *endo*-linked species been suggested based on the basis of other characterization (although we have previously calculated[4] that energy differences between *exo,exo*, *exo,endo*, and *endo,endo* isomers of [RhCp$_2$]$_2$ are only a few kJ mol^{-1}).

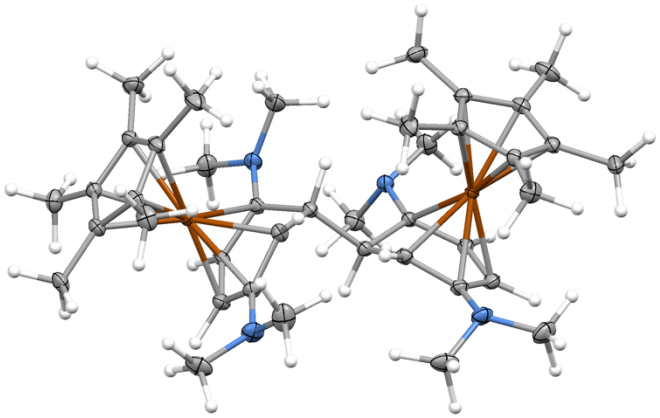

Fig. 4. Molecular structure of **4$_2$b** (50% thermal ellipsoids) determined by X-ray crystallography.

As in other dimers of 19-electron species, such as **2$_2$**, the central C—C bonds in both **4$_2$a** and **4$_2$b** are rather long (Table 2).[4] We have previously found that these bond lengths do not generally correlate well with bond dissociation energetics,[4] which also depend on the stability of the 19-electron monomers. Table 2 shows that the two isomers of **4$_2$** show generally similar Ru—C bond lengths to **2$_2$**; however, in **4$_2$a** and the *exo*-connected monomer of **4$_2$b** the bonds from Ru to the amino-substituted C atom adjacent to the position of dimerization are rather long, similar to the Ru—CN bond lengths in **3**$^+$ and **4**$^+$ structures (Table S1, †ESI). Table 2 also shows that the η^5-cyclohexadienyl ligands are folded from planarity in a similar way to those in **2$_2$**, regardless of whether they are connected through an *exo* or *endo* linkages. The amino substituents are generally more pyramidal than those in the amino-substituted RuCp*(arene) cations: Σ(C-N-C) values of 346.5 and 349.3° are seen for **4$_2$a**, which can be compared to values of 336.9-354.2° for **4$_2$b** and 354.1-358.8° for **I**$^+$, **3**$^+$, **4**$^+$ (Table S1, †ESI). The amino groups in the dimers are also generally less coplanar with the π-systems to which they are attached than those of the cations, suggesting that they do not act as particularly effective π-donors in the dimers.

Reactivity of [RuCp*(1,4-(Me$_2$N)$_2$C$_6$H$_4$)]$_2$ isomers

Table 1 compares the values of E(D$_2^+$/D$_2$) obtained from the irreversible oxidation peaks observed in the cyclic voltammograms of **4$_2$a** and **4$_2$b** (**4$_2$b**/**4$_2$c** mixtures show similar voltammograms to pure **4$_2$b**, suggesting that **4$_2$c** is oxidized at similar potential to **4$_2$b**) to the corresponding values for **1$_2$** and **2$_2$** (see Fig. S2 †ESI). We examined the solution rates of reaction of these dimers with 1,13-bis(triisopropylsilylethynyl)pentacene (TIPS-pentacene, **IV**, Fig. 5) as a measure of the relative reactivity of these species. We have previously found that **1$_2$** and **2$_2$** react with **IV** ($E_{1/2}^{0/-}$ = –1.45 V, $E_{1/2}^{-/2-}$ = –1.93 V[48]) through endergonic electron transfer (ET), followed by cleavage of D$_2^{\bullet+}$ and a second ET to another **IV** molecule from the neutral monomer. In contrast, [RhCp*Cp]$_2$ reacts by both this "ET-first" mechanism and a "cleavage-first" mechanism, in which endergonic dissociation of D$_2$ gives two 19-electron monomers which then undergo exergonic ET reactions with **IV**. The difference in reactivity between these two dimers reflects very different dissociation energetics (DFT calculations give ΔG_{diss} = +132.3 and +1.8 kJ mol^{-1} for **2$_2$** and [RhCp*Cp]$_2$, respectively, in continuum dielectric representing THF).[48] Similar differences in mechanism are also seen between organic dimers with different dissociation energies.[24]

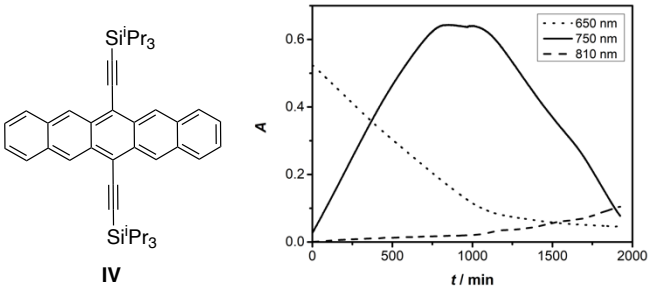

Fig. 5. Left: structure of TIPS-pentacene. Right: Evolution of absorbance at 650, 750, and 810 nm, corresponding to absorption maxima for **IV**, **IV**$^{\bullet-}$, and **IV**$^{2-}$, respectively, for the reaction of **IV** with excess **4$_2$b** in chlorobenzene. See also Fig. S12, †ESI.

The E(D$_2^+$/D$_2$) value for **4$_2$a** is the most reducing we have yet observed for a dimer of a 19-electron sandwich compound, consistent with the observed air sensitivity of this isomer; this potential is more cathodic than both the corresponding value for [RhCp*Cp"]$_2$ (–1.29 V)[4] and the oxidation potential of CoCp$_2$ (–1.33 V), both of which are also air sensitive. The ease of oxidation also means that direct ET from **4$_2$a** to TIPS-pentacene is only slightly endergonic (ΔG_{ET} = ca. +4 kJ mol^{-1}). Indeed in chlorobenzene **4$_2$a** reacts much more rapidly with **IV** than **1$_2$**/**2$_2$** (ΔG_{ET} = +35-38 kJ mol^{-1}). Indeed, as in the case of [RhCp*Cp"]$_2$ (ΔG_{ET} = +15 kJ mol^{-1}), the reaction to form **IV**$^{\bullet-}$ is essentially complete (at D$_2$ and **IV** concentrations of 1.5 × 10^{-3} and 1.5 ×10^{-4} M, respectively) before the cuvette can be transferred from the glove-box to the spectrometer, precluding determination of reaction kinetics in solution by vis-NIR spectroscopy.‡ At longer reaction times, the **IV**$^{\bullet-}$ absorption features drop irregularly and irreproducibly in absorbance, presumably due to precipitation, and in some experiments absorptions attributable to formation of **IV**$^{2-}$ (presumably also via "ET-first" pathway, but with a more endergonic initial step) are seen.

On the other hand, **4$_2$b** is *less* easily oxidized than **1$_2$** or **2$_2$**. Accordingly, reaction with **IV** by the "ET-first" mechanism is expected to be slow; indeed, the E_{ox}(D$_2^+$/D$_2$) potential for **4$_2$b** is the same as that measured for the most easily oxidized isomer of [IrCp*Cp]$_2$, which does not react detectably with **IV** in the dark in chlorobenzene.[32] The reactions of **4$_2$b** or **4$_2$b**/**4$_2$c** mixtures with **IV** *are* found to be relatively slow and, moreover, to proceed primarily via the "cleavage-first", rather than "ET-first", mechanism, which is unprecedented for a [RuCp*(arene)]$_2$ derivative, but consistent with the relatively anodic value of E_{ox}(D$_2^+$/D$_2$), which would be expected to lead to

very slow reaction via the "ET-first"pathway, and the relatively low DFT-calculated ΔG_{diss} values for these isomers (see following section), which favor the "cleavage-first" pathway. Specifically, with excess dimer, the absorbance of $\mathbf{IV}^{\bullet-}$ increases in roughly linear fashion with time, indicating a rate law that is zero order in **IV**, reaches a maximum, and then decreases with a comparable slope as absorption features characteristic of $\mathbf{IV}^{2-}$ appear (as expected since a rate-determining cleavage step would be independent of which species is subsequently reduced, Fig. 5). The rate constant, *k*, defined as:

$$d[\mathbf{IV}]dt = -2d[\mathbf{4_2b}/\mathrm{dt}] = 2k[\mathbf{4_2b}] \qquad (2)$$

can be estimated as ca. 10^{-6} s^{-1}, ca. two orders-of-magnitude lower than determined for $[RhCp^*Cp]_2$, indicating a higher barrier to $\mathbf{4_2b}$ than in $[RhCp^*Cp]_2$, qualitatively consistent with differences in DFT-calculated ΔG_{diss} values (see below).

Quantum-chemical calculations

To gain more insight into the properties of the isomers of $\mathbf{4_2}$ discussed above, calculations were performed at the M06/6–31G**/LANL2DZ DFT level for the dimer isomers shown in Scheme 5, the corresponding dimer cations, and on the monomeric neutral and cationic species, using a continuum dielectric to model solvation by THF.

The DFT-optimized structure for $\mathbf{4}^+$ reproduces the arene fold, while that for the neutral **4** monomer exhibits a much larger distortion of the arene ring from planarity, and a large spin density on the CH carbon atom most distant from the metal, which may, along with steric effects, help kinetically favor dimerization through the CH positions (see further discussion in section S7 and Fig. S13, †ESI). The optimized molecular structures of the dimers $\mathbf{4_2a}$ and $\mathbf{4_2b}$ are close to those seen in the crystal structures, for example, qualitatively reproducing the differences in the central C—C bond lengths between the two isomers (compare Tables X and SY).

The IE of **4** in a dielectric continuum modelling THF was calculated to be a little lower than that for **2** (Table 3),[48] somewhat underestimating the difference in $E_{red}(D^+/D)$ values shown in Table 2.

Table 3. DFT-Calculated Characteristics of RuCp*(arene) Dimers in Dielectric Continuum Representing THF

D_2		structure [a]		G_{rel} [b] / kJ mol^{-1}	IE(D$^\bullet$) / eV	IE(D_2) / eV	$\Delta G_{diss}(D_2)$ / kJ mol^{-1}	$\Delta G_{diss}(D_2^{\bullet+})$ / kJ mol^{-1}	$E(D^+/0.5D_2)$ [c] / V
$\mathbf{2_2}$ [d]	–	*exo*,*exo*-CHCH	C_{2h}	–	2.10	4.03	+132.3	–26.8	–2.01
$\mathbf{4_2}$	**a**	*exo*,*exo*-CHCH	C_i	0	2.00	3.61	+95.3	–42.9	–2.40
	–	*exo*,*exo*-CHCH	C_2	+1.9		3.71	+93.4	–48.6	–2.41
	–	*exo*,*exo*-CHCN	C_1	+43.3		3.06	+52.0	–9.3	–2.62
	–	*exo*,*exo*-CNCN	C_{2h}	+114.2		2.34	–18.9	–12.4	–
	b	*exo*,*endo*-CHCH	C_1	+24.7		3.99	+70.6	–103.4	–2.52
	c	*exo*,*endo*-CHCH	C_1	+40.2		3.97	+55.1	–112.2	–2.61

[a] See Scheme 5. [b] Relative free energies of different isomers of $\mathbf{4_2}$. [c] Estimated using Eq. 1 using experimental $E(D^+/D)$ values from Table 2 and the DFT ΔG_{diss} values. [d] Data from ref. 48.

In principle, considering only dimerization through the arene rings and not through the Cp* groups, 13 regio- and diastereoisomers are possible for $\mathbf{4_2}$ (see Fig. S14, †ESI for the full set). For *exo*,*exo*-dimers there are in principle four such isomers (Scheme 5). The crystal structure of $\mathbf{4_2b}$ clearly shows that *exo*,*endo* isomers also have to be considered and five such isomers are in principle possible: the CH–CH linked isomers (corresponding to $\mathbf{4_2b}$ and $\mathbf{4_2c}$); a $C(NMe_2)$–$C(NMe_2)$ linked structure; and two $C(NMe_2)$–CH linked diastereomers. Finally, four *endo*,*endo* analogues of the four *exo*,*exo* species are possible. Table 4 shows quantities calculated for the key examples shown in Scheme 5. The C_i $\mathbf{4_2a}$ structure is the lowest in energy of the *exo*,*exo* isomers, but the C_2 isomer is very close in energy, although not observed in our experimental work. The CH–$C(NMe_2)$ linked *exo,exo* isomer, however, is calculated to be much higher in energy than $\mathbf{4_2a}$, suggesting a strong thermodynamic preference for forming CH—CH linkages in addition to the kinetic effects of the spin-density distribution in **4**.

The free energies of the two CH—CH linked *exo*,*endo* isomers, corresponding to $\mathbf{4_2b}$ and $\mathbf{4_2c}$, relative to that of $\mathbf{4_2a}$ indicate the *endo* linkage has an effect on energy of the isomer smaller than or comparable to that of a bridgehead NMe_2. We extrapolate that the other structures (*exo,endo* and with one or more amino-bridgehead substituent or *endo,endo*) are likely high in energy.

Table 4 also compares key energetic parameters relating to the reactivity of $\mathbf{2_2}$ and some isomers of $\mathbf{4_2}$. The IE values for the dimers model their electrochemically determined $E_{ox}(D_2^+/D_2)$ values and are relevant to their air-stability and their reactivity via the "ET-first" mechanism. Consistent with the electrochemical data, the DFT calculations indicate that $\mathbf{4_2a}$ (as well as its related C_2 stereoisomer) is much more easily oxidized than $\mathbf{4_2b}$ and $\mathbf{4_2c}$; however, the calculations underestimate the experimental difference in redox potentials and suggest $\mathbf{4_2b}$ should be more easily ionized than $\mathbf{2_2}$. However, the two *exo,exo* species with CH—$C(NMe_2)$ or CH—$C(NMe_2)$ linkages are calculated to have *much* lower IEs even than $\mathbf{4_2a}$, suggesting that even if it were possible to form these species they would be extremely reactive and air sensitive.

The free energies of dissociation, ΔG_{diss}, are relevant to the feasibility of reaction via the "cleavage-first" mechanism. There is considerable variation in calculated ΔU_{diss} (Table S2, †ESI) and ΔG_{diss} (Table 3) values between the different isomers of $\mathbf{4_2}$, necessarily identical to the variation in the energies of the isomers. In particular, values for $\mathbf{4_2a}$ are lower than for $\mathbf{1_2}$ and $\mathbf{2_2}$, with values for $\mathbf{4_2b}$ and $\mathbf{4_2c}$ being lower still, although still considerably larger than the values

for $[RhCp^*Cp]_2$ (+1.8 kJ mol^{-1}),[48] qualitatively consistent with the observation that **4_2b**/**4_2c** appear to react with TIPS-pentacene via a dissociative mechanism, but more slowly than $[RhCp^*Cp]_2$.

In previous work we estimated the overall thermodynamic reducing strength of dimers, $E(D^+/0.5D_2)$, according to eq. 1 where $E(D^+/D^\bullet)$ is measured electrochemically and ΔG_{diss} is taken from DFT calculations (although for $[RhCp^*Cp]_2$ we have been able to obtain experimental estimates from dissociation and dimerization rate constants,[36] or in an organic case, from ESR spectroscopy[24]). For **4_2a**, the dopant is calculated to be more reducing than **2_2** (or **1_2**) due to *both* a more reducing value of $E(D^+/D^\bullet)$ *and* to a significantly weaker central C—C bond. For the other isomers of **4_2**, the central C—C bonds are even weaker and accordingly the dimers are even stronger reductants in a thermodynamic sense. Of particular interest, the values of $E(D^+/0.5D_2)$ for **4_2b** and **4_2c** are the most reducing yet obtained for isolable dimers of this type, substantially exceeding even the values of –2.14 and –2.15 V estimated for one of the isomers of $[IrCp^*Cp]_2$ and for $[RhCp^*Cp'']_2$ respectively.[4]

As in previous computational investigations of dimer reactivity,[3,4,24,48] the dimer cations are, in each case, calculated to undergo dissociation much more readily than their neutral counterparts, consistent with the irreversible oxidations observed for the dimers and with the assumption that the second step of the "ET-first" mechanism, dissociation of $D_2^{\bullet+}$, is rapid.

Fig. 6 shows the HOMO and HOMO–1 wavefunctions for **4_2a** and **4_2b**. Those for **4_2a** are similar to those for other *exo,exo* organometallic dimers including **1_2**:[4] they can be regarded respectively as in-phase and out-phase combinations of the HOMOs of two RuCp*(η^5-pentadienyl) fragments, the HOMO being substantially destabilized by out-of-phase contributions the σ bonding orbital associated with the central C—C bond. In contrast, HOMO and HOMO–1 for **4_2b** are localized on the *exo*- and *endo*-connected monomers respectively, there is a smaller energetic separation between them than in **4_2a**, and the HOMO is lower in energy than in **4_2a** (consistent with IE data in Table 3 and D_2^+/D_2 redox potentials in Table 1) The localization is due to both the inequivalence of the two monomer units, and a weaker electronic coupling between the two sites (see section S6 of the ESI for additional discussion).

Experimental

Materials and methods

All commercially available chemicals were used without further purification unless otherwise noted. The synthesis and purification of dimers were performed under an atmosphere of nitrogen using standard Schlenk techniques or in a glove box. THF, Et_2O, and MeCN were dried using a solvent purification system from MBraun, while chlorobenzene was dried using CaH_2. Mass spectra were measured on an Applied Biosystems 4700 Proteomics Analyzer using ESI mode. Elemental analyses were carried out by Atlantic Microlabs using a LECO 932 CHNS elemental analyzer). Electrochemical characterization was performed in 0.1 M Bu_4NPF_6 in dry THF under nitrogen at a scan rate of 50 or 100 mV s^{-1}. A CH Instruments 620D potentiostat was used with a three-electrode system: a glassy carbon working electrode, a platinum wire auxiliary electrode, and a silver wire anodized in 1 M aqueous potassium chloride solution as a pseudo-reference electrode. Ferrocene was used as an internal reference. Solution doping vis.-NIR studies of reactivity were performed in chlorobenzene solutions 1.5×10^{-4} M in **IV** and 1.5×10^{-3} in **4_2**. The solutions were prepared in a N_2-atmosphere glove-box and transferred to the spectrometer in 1 cm air-tight cuvettes.

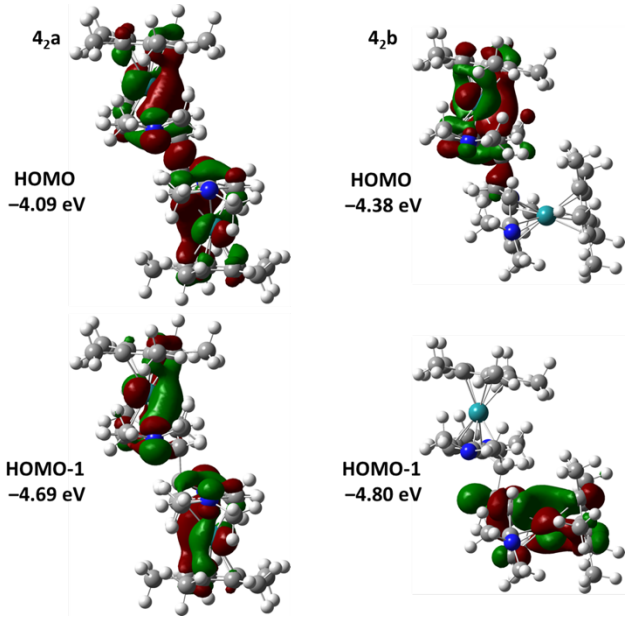

Fig. 6. HOMO and HOMO–1 of **4_2a** (left) and **4_2b** (right).

Synthesis and characterization

General procedure for $[RuCp^*(arene)]^+PF_6^-$. $[RuCp^*(NCMe)_3]^+PF_6^-$ [49] (2.00 g, 4.0 mmol) was added to a deoxygenated solution of the appropriate arene (ca. 30 mmol) in 1,2-dichloroethane (20 mL) and; the mixture was heated to reflux for 24 h. The solvent was removed under reduced pressure and the resulting brown precipitates were dissolved in acetone and passed through a plug of alumina. Acetone was removed under reduced pressure and the residue was recrystallized from CH_2Cl_2/Et_2O.

$[RuCp^*(1\text{-}(Me_2N)\text{-}3,5\text{-}Me_2C_6H_3)]^+PF_6^-$ ($3^+PF_6^-$). Obtained using the general procedure as a white solid (1.59 g, 75%) from $[RuCp^*(NCMe)_3]^+PF_6^-$ (2.00 g, 4.0 mmol) and 1-dimethylamino-3,5-dimethylbenzene (4.14 g, 27.7 mmol). ^1H NMR (500 MHz, acetone-d_6): δ 5.59 (s, 2H, arene 2,6-C*H*), 5.47 (s, 1H, arene 4-C*H*), 3.06 (s, 6H, NMe_2 CH_3), 2.21 (s, 6H, CMe CH_3), 1.95 (s, 15H, Cp* CH_3). $^{13}C\{^1H\}$ NMR (136 MHz, acetone-d_6): 127.92, 99.22, 94.11, 85.60, 71.41, 40.08, 19.07, 10.77. Anal. Calcd. for $C_{20}H_{30}F_6PNRu$: C, 45.28; H, 5.70; N, 2.64. Found: C, 45.49; H, 5.72; N, 2.69. MS (ESI) *m/z* 386.3 ($[M–PF_6]^+$).

[RuCp*(1,4-(Me$_2$N)$_2$C$_6$H$_4$)]$^+$PF$_6^-$ (4$^+$PF$_6^-$). Obtained using the general procedure as a blue-gray solid (1.16 g, 53%) from [RuCp*(NCMe)$_3$]$^+$PF$_6^-$ (2.00 g, 4.0 mmol) and 1,4-bis(dimethylamino)benzene (4.56 g, 27.7 mmol). ^{1}H NMR (500 MHz, chloroform-*d*): δ 5.18 (s, 4H, arene C*H*), 3.01 (s, 12H, NMe$_2$, C*H*$_3$), 2.03 (s, 15H, Cp* C*H*$_3$). Anal. Calcd. for $C_{20}H_{31}F_6PN_2Ru$: C, 44.04; H, 5.73; N, 5.14. Found: C, 43.81; H, 5.77; N, 5.24. MS (ESI) *m/z* calcd. for $C_{20}H_{31}N_2Ru^+$ ([M–PF$_6$]$^+$): 401.1517; found: 401.1520.

[RuCp*(1,4-(Me$_2$N)$_2$C$_6$H$_4$)]$_2$ (4$_2$). A suspension of **4**$^+$PF$_6^-$ (2.00 g, 3.66 mmol) in anhydrous THF (400 mL) was added to an excess of NaK$_2$-SG(I) (3.17 g, equivalent to ca. 33 mmol alkali metal) under inert atmosphere. The reaction was stirred for 75 min at room temperature, during which time the suspension turned from a blueish to green-yellowish color. The solution was then transferred via cannula under inert atmosphere from the remaining NaK2-SG(1) (which was subsequently quenched by sequential slow addition of isopropanol, ethanol, and water.). The solution was filtered through Celite®, and evaporated under reduced pressure. The solid residue was extracted into copious Et$_2$O, filtered again through Celite®, evaporated under reduced pressure, and dried under vacuum. The solid was washed with MeCN (3 × 10 mL) to remove traces of 1,4-(Me$_2$N)$_2$C$_6$H$_4$ and again dried under vacuum to afford a mixture of isomers of **4$_2$** as a yellow solid (980 mg, 68%). Anal. Calcd. for $C_{40}H_{62}N_4Ru_2$: C, 59.97; H, 7.80; N, 6.99. Found: C, 60.78; H, 8.03; N, 6.64. MS (ESI) *m/z* calcd. for $C_{20}H_{31}N_2Ru^+$ ([M/2]$^+$): 401.1517; found: 401.1525. The isomeric mixture was further separated by washing quickly with a small quantity of Et$_2$O (3 × 10 mL), leaving a solid that was found to be essentially pure isomer **4$_2$a** (up to ca. 380 mg, depending on washing time, representing ca. 40% of the total dimer).

The filtrate was then evaporated under reduced pressure and exposed to air for 30 min to decompose a remaining small proportion of **4$_2$a**; this solid was then washed (in a glove box) with MeCN (4 × 10 mL) and dried under vacuum to afford a ca. 2:1 **4$_2$b/4$_2$c** mixture (ca. 550 mg, ca. 56% of total dimer). These isomers proved challenging to separate further in bulk, although the proportion of **4$_2$b** in the mixture could be slightly increased by further washing with MeCN. However, a very small relatively pure sample of **4$_2$b** was isolated in from one reaction by multiple washings with MeCN. An even smaller relatively pure sample of **4$_2$c** was obtained adventitiously on one occasion, when a small quantity of solid precipitated from the MeCN washings.

For assignments of the NMR data given below (based on COSY, HSQC, HMBC, and NoE spectra) see Fig. S4-6 in the †ESI.

Data for 4$_2$a. Anal. Calcd. for $C_{40}H_{62}N_4Ru_2$: C, 59.97; H, 7.80; N, 6.99 Found: C, 60.62; H, 8.23; N, 6.13. ^{1}H NMR (500 MHz, benzene-d$_6$): δ 4.53 (dd, *J* = 5.5, 1.5 Hz, 2H), 3.74 (d, *J* = 5.5 Hz, 2H), 2.52 (s, 12H), 2.49 (m, 2H), 2.46 (s, 12H), 2.49 (m, 1H), 1.85 (s, 30H). ^{13}C{^{1}H} NMR (176 MHz, benzene-*d*$_6$): δ 115.04, 86.62, 85.76, 64.27, 57.90, 54.09, 42.17, 40.11, 25.33, 13.92.

Data for 4$_2$b. ^{1}H NMR (700 MHz, toluene-*d*$_8$): δ 4.44 (dd, *J* = 5.6, 1.4 Hz, 1H), 4.38 (dd, *J* = 5.6, 1.4 Hz, 1H), 3.99 (d, *J* = 5.6 Hz, 1H), 3.75 (dd, *J* = 5.6, 1.4 Hz, 1H), 3.70 (ddd, *J* = ca. 8.4, ca. 6.5, < 1 Hz, 1H), 2.77 (dd, *J* = 6.3, < 1 Hz, 1H), 2.62 (s, 6H), 2.55 (s, 1H), 2.44 (s, 6H), 2.39 (s, 6H), 2.36 (s, 6H), 2.29 (d, *J* = 9.1 Hz, 1H), 1.94 (s, 15H), 1.87 (s, 15H). ^{13}C{^{1}H} NMR (176 MHz, toluene-*d*$_8$): δ 119.91, 114.19, 87.40, 87.08, 83.10, 73.23, 72.30, 65.39, 61.91, 59.91, 59.47, 45.92, 45.76, 43.12, 41.63, 41.15, 30.15, 23.84, 13.42, 12.89.

Data for 4$_2$c. ^{1}H NMR (500 MHz, benzene-*d*$_6$): δ: 4.61 (dd, J = 5.5, 2 Hz, 1H), 4.45 (dd, J$_1$ = 5.5, 2 Hz, 1H), 3.96 (d, *J* = 5 Hz, 1H, **3**), 3.61 (dd, J$_1$ = 5.5, 2.5 Hz, 1H, **4**), 3.48 (ddd, J = 8.5, 6.5, 2.0 Hz, 1H, **5**), 2.89 (dd, J$_1$ = 7, 2 Hz, 1H, **6**), 2.66 (s, br, 6H), 2.61 (m, 1H), 2.53 (s, 6H), 2.50 (s, 6H), 2.42 (m, 1H), 2.15 (s, 6H), 2.09 (s, 15H), 1.94 (s, 15H). ^{13}C{^{1}H} NMR (126 MHz, benzene-*d*$_6$): δ 117.33, 112.20, 90.04, 86.99, 86.32, 74.88, 66.42, 62.7, 61.24, 58.73, 53,24, 46.34, 42.88, 41.14, 39.80, 25.79, 21.15, 13.21, 11.21. ^{13}C{^{1}H} NMR (176 MHz, toluene-*d*$_8$) δ 119.91, 114.19, 87.40, 87.08, 83.10, 73.23, 72.30, 65.39, 61.91, 59.91, 59.47, 45.92, 45.76, 43.12, 41.63, 41.15, 30.15, 23.84, 13.42, 12.89.

Crystal structure determinations

X-ray diffraction data were collected on a three-circle Bruker APEX-II CCD diffractometer in φ and ω scan mode (**3**$^+$PF$_6^-$ and **4**$^+$PF$_6^-$), or using ω scans on a 4-four--circle XtaLab Synergy, Dualflex, HyPix diffractometer (**4$_2$a** and **4$_2$b**), in each case at *T* = 100 K and employing MoK_α-radiation (λ = 0.71073 Å). Key parameters relating to crystal structure determinations are summarized in Table 4. Further crystallographic details have been deposited in CIF format with the Cambridge Crystallographic Data Center (Table 5); these can be obtained free of charge from the via www.ccdc.cam.ac.uk/data_request/cif. Figures showing the atomic numbering schemes are given in the †ESI (Figs S15-18).

Quantum-chemical calculations

Density functional theory (DFT) calculations were carried out at the M06/6-31G(d,p)/LANL2DZ level using the Gaussian09 (Revision E.01) software suite.[50-56] The influence of the solvent environment (tetrahydrofuran, THF; ε = 7.43) was modelled through the polarizable continuum model. Optimized geometries were confirmed to be minima on the potential energy surface through normal mode analyses.

Table 4. Details of crystal structure determinations

	3$^{+}PF_6^{-}$	**4**$^{+}PF_6^{-}$	**4_2a**	**4_2b**
formula	$C_{20}H_{30}F_6NPRu$	$C_{20}H_{31}F_6N_2PRu$	$C_{40}H_{62}N_4Ru_2$	$C_{40}H_{62}N_4Ru_2$
M	530.49	545.51	801.07	801.07
crystal system	Monoclinic	monoclinic	monoclinic	triclinic
space group	*C*2/*c*	$P2_1/c$	$P2_1/c$	*P*–1
a / Å	39.310(7)	7.343(2)	14.2873(4)	10.6226(1)
b / Å	7.127(1)	17.294(4)	8.6243(2)	12.2061(2)
c / Å	16.505(3)	17.914(4)	15.3075(4)	15.1648(1)
α / °	90	90	90	89.304(1)
β / °	113.299(3)	100.443(3)	105.410(3)	79.584(1)
γ / °	90	90	90	72.407(1)
V / Å^3	4347.0(13)	2237.3(9)	1818.35(9)	1841.53(4)
Z	8	4	2	2
reflections measured	21940	23254	18861	55488
independent reflections, R_{int}	6342, 0.0589	3971, 0.0695	18861, –	17857, 0.0403
observd reflections ($I > 2\sigma(I)$)	4744	3310	14694	15504
$R(F)$ ($I > 2\sigma(I)$)	0.0489	0.0525	0.0510	0.0251
$wR(F^2)$ (all data)	0.1089	0.1135	0.1546	0.0586
CCDC #	2079705	2080755	2083852	2083960

Conclusions

Reduction of [RuCp*(1,4-$(Me_2N)_2$-C_6H_4)]$^+$, **4**$^+$, leads to formation of a mixture of isomers of **4_2**. One of these, **4_2a**, has a molecular structure similar to that of other group 8 [MCp(arene)]$_2$ dimers, with a central C—C bond on the opposite face of the arene ligand to the metal (*exo*,*exo* linkage). The NMe_2 substituents result in a more reducing values of both $E(D^+/D)$ and $E(D^+/0.5D_2)$ than for **1_2** or **2_2**, but also in a much more reducing value of $E(D_2^{\bullet+}/D_2)$, which in turn renders this dimer highly unstable to air. On the other hand, **4_2b** and **4_2c** are *exo*,*endo* dimers; they are the first examples of dimers of 19-electron sandwich compounds in which the central C—C bond is on the same face of one or both linked ligands. The *exo,endo* linkage leads to an unusual combination of properties; these isomers are less easily oxidized, and therefore more stable to air, than **1_2** or **2_2**, while exhibiting lower dissociation energies, which, in combination with the $E(D^+/D)$ value, result in strong thermodynamic reducing ability. Indeed, the $E(D^+/0.5D_2)$ values estimated from a combination of electrochemical and DFT data for **4_2b** and **4_2c** are more reducing than those of other dimers of 19-electron sandwich compounds and of [Y-DMBI]$_2$ dimers.[4,24,57] On the other hand, the formation of these relatively stable, yet highly reducing, dimers is accompanied by that of the much less stable, but less reducing, **4_2a** isomer, complicating their isolation and lowering the yield in which they can be obtained. In any case, regardless of the practicality of these particular compounds, their properties demonstrate for the first time that *exo*,*endo*-linked dimers can have quite different properties from those of their *exo*,*exo* counterparts. If *exo*,*endo* and *endo*,*endo* dimers, especially the counterparts of relatively strongly bound *exo*,*exo* species, can be intentionally and selectively obtained, they may be useful n-dopants for organic semiconductors, expanding the range of properties currently available, and perhaps as reducing agents in other contexts.

Author Contributions

Conceptualization, E.L., K.M., S.R.M., and S.B.; Investigation, E.L., C.R., J.B., V.K., S.R., K.M.; Writing – Original Draft, E.L. and S.B.; Writing – Review and Editing, all authors. Funding Acquisition, C.R., T.V.T., S.R.M. and S.B. Supervision, T.V.T., S.R.M., and S.B.

Conflicts of interest

There are no conflicts to declare.

Acknowledgements

This work was supported by the National Science Foundation through DMR-1305247 and DMR-1807797 and the RUDN University Strategic Academic Leadership Program. The work at the University of Kentucky was supported by the Office of Naval Research Young Investigator Program (Award No. N00014-18-1-

2448), with supercomputing resources provided by the University of Kentucky Information Technology Department and Center for Computational Sciences (CCS).

Notes and references

‡ At longer reaction times the absorbance decreases erratically, likely due to precipitation, either of $\mathbf{4^{+}IV^{\bullet-}}$ or perhaps of $(\mathbf{4^{+}})_2\mathbf{IV^{2-}}$ Redox potentials in THF / NBu_4PF_6 suggest ΔG_{ET} for formation of $\mathbf{IV^{2-}}$ to be ca. +50 kJ mol^{-1}, but the separation of 1st and 2nd redox potentials is often highly solvent and electrolyte dependent,[58] and Coulombic interactions in the precipitate may further drive the reaction.

1. O. V. Gusev, M. A. Ievlev, M. G. Peterleitner, S. M. Peregudova, L. I. Denisovich, P. V. Petrovskii and N. A. Ustynyuk, *J. Organomet. Chem.*, 1997, **534**, 57.
2. O. V. Gusev, M. A. Ievlev, T. A. Peganova, M. G. Peterleitner, P. V. Petrovskii, Y. F. Oprunenko and N. A. Ustynyuk, *J. Organomet. Chem.*, 1998, **551**, 93.
3. S. Guo, S. B. Kim, S. K. Mohapatra, Y. Qi, T. Sajoto, A. Kahn, S. R. Marder and S. Barlow, *Adv. Mater.*, 2012, **24**, 699.
4. S. K. Mohapatra, A. Fonari, C. Risko, K. Yesudas, K. Moudgil, J. H. Delcamp, T. V. Timofeeva, J.-L. Brédas, S. R. Marder and S. Barlow, *Chem. Eur. J.*, 2014, **20**, 15385.
5. Y. Qi, S. K. Mohapatra, S. B. Kim, S. Barlow, S. R. Marder and A. Kahn, *Appl. Phys. Lett.*, 2012, **100**, 083305.
6. S. Olthof, S. K. Mohapatra, S. Barlow, S. Mehraeen, V. Coropceanu, J.-L. Brédas, S. R. Marder and A. Kahn, *Phys. Rev. Lett.*, 2012, **109**, 176601.
7. S. Olthof, S. Singh, S. K. Mohapatra, S. Barlow, S. R. Marder, B. Kippelen and A. Kahn, *Appl. Phys. Lett.*, 2012, **101**, 253303.
8. Y. Zhang, H. Phan, H. Zhou, X. Zhang, J. Zhou, K. Moudgil, S. Barlow, S. R. Marder, A. Facchetti and T.-Q. Nguyen, *Adv. Electron. Mater.*, 2017, **3**, 1600546.
9. E. Perry, C.-Y. Chiu, K. Moudgil, R. Schlitz, C. Takacs, K. O'Hara, J. Labram, A. Glaudell, J. Sherman, S. Barlow, C. J. Hawker, S. R. Marder and M. L. Chabinyc, *Chem. Mater.*, 2017, **29**, 9742.
10. H.-I. Un, S. A. Gregory, S. K. Mohapatra, M. Xiong, E. Longhi, Y. Lu, S. Rigin, S. Jhulki, C.-Y. Yang, T. V. Timofeeva, J.-Y. Wang, S. K. Yee, S. Barlow, S. R. Marder and J. Pei, *Adv. Energy Mater.*, 2019, **9**, 1900817.
11. X. Lin, B. Wegner, K. M. Lee, M. A. Fusella, F. Zhang, K. Moudgil, B. P. Rand, S. Barlow, S. R. Marder, N. Koch and A. Kahn, *Nat. Mater.*, 2017, **16**, 1209.
12. A. J. Giordano, F. Pulvirenti, T. M. Khan, C. Fuentes-Hernandez, K. Moudgil, J. H. Delcamp, B. Kippelen, S. Barlow and S. R. Marder, *ACS Appl. Mater. Interf.*, 2015, **7**, 4320.
13. R. Schlesinger, S. Blumstengel, C. Christodoulou, R. Ovsyannikov, B. Kobin, K. Moudgil, S. Barlow, S. Hecht, S. R. Marder, F. Henneberger and N. Koch, *Nat. Commun.*, 2015, **6**, 6754.
14. A. R. Kirmani, A. Kiani, M. M. Said, O. Voznyy, N. Wehbe, G. Walters, S. Barlow, E. H. Sargent, S. R. Marder and A. Amassian, *ACS Energy Lett.*, 2016, **1**, 922.
15. A. E. Mansour, M. M. Said, S. Dey, H. Hu, S. Zhang, R. Munir, Y. Zhang, K. Moudgil, S. Barlow, S. R. Marder and A. Amassian, *Adv. Funct. Mater.*, 2017, **27**, 1602004.
16. F. Zhang, C. Klein, E. Longhi, S. Barlow, S. R. Marder, G. Sarusi and A. Kahn, *Chem. Mater.*, 2019, **31**, 6624.
17. R. Guo, Q. Li, Y. Zheng, B. Lei, H. Sun, Z. Hu, J. Zhang, L. Wang, E. Longhi, S. Barlow, S. R. Marder, J. Wang and W. Chen, *Mater. Today*, 2019, **30**, 26.
18. T. Schultz, D. Lungwitz, E. Longhi, S. Barlow, S. R. Marder and N. Koch, *Adv Funct. Mater.*, 2021, **31**, 2010174.
19. S. A. Paniagua, J. Baltazar, H. Sojoudi, S. K. Mohapatra, S. Zhang, C. L. Henderson, S. Graham, S. Barlow and S. R. Marder, *Mater. Horiz.*, 2014, **1**, 111.
20. A. Higgins, S. K. Mohapatra, S. Barlow, S. R. Marder and A. Kahn, *Appl. Phys. Lett.*, 2015, **106**, 163301.
21. K. Akaike, M. V. Nardi, M. Oehzelt, J. Frisch, A. Opitz, C. Christodoulou, G. Ligorio, P. Beyer, M. Timpel, I. Pis, F. Bondino, K. Moudgil, S. Barlow, S. R. Marder and N. Koch, *Adv. Funct. Mater*, 2016, **26**, 2493.
22. M. Geier, K. Moudgil, S. Barlow, S. R. Marder and M. C. Hersam, *Nano Lett.*, 2016, **16**, 4329.
23. B. D. Naab, S. Zhang, K. Vandewal, A. Salleo, S. Barlow, S. Marder and Z. Bao, *Adv. Mater.*, 2014, **26**, 4268.
24. S. Zhang, B. D. Naab, E. V. Jucov, S. Parkin, E. G. B. Evans, G. L. Millhauser, T. V. Timofeeva, C. Risko, J.-L. Brédas, Z. Bao, S. Barlow and S. R. Marder, *Chem. Eur. J.*, 2015, **21**, 10878.
25. B. D. Naab, X. Gu, T. Kurosawa, J. W. F. To, A. Salleo and Z. Bao, *Adv. Electron. Mater.*, 2016, **2**, 1600004.
26. D. Yuan, D. Huang, C. Zhang, Y. Zou, C.-a. Di, X. Zhu and D. Zhu, *ACS Appl. Mater. Interf.*, 2017, **9**, 28795.
27. J. L. Schrenk, A. M. McNair, F. B. McCormick and K. R. Mann, *Inorg. Chem.*, 1986, **25**, 3501.
28. P. J. Fagan, M. D. Ward and J. C. Calabrese, *J. Am. Chem. Soc.*, 1989, **111**, 1698.
29. C. Gemel, K. Mereiter, R. Schmid and K. Kirchner, *Organometallics*, 1996, **15**, 532.
30. M. E. Navarro Clemente, P. Juárez Saavedra, M. Cervantes Vásquez, M. A. Paz-Sandoval, A. M. Arif and R. D. Ernst, *Organometallics*, 2002, **21**, 592.
31. L. Quebatte, R. Scopelliti and K. Severin, *Eur. J. Inorg. Chem.*, 2006, 231.
32. S. K. Mohapatra, A. Romanov, T. V. Timofeeva, S. R. Marder and S. Barlow, *J. Organomet. Chem.*, 2014, **751**, 314.
33. A. I. Konovalov, E. O. Gorbacheva, F. M. Miloserdov and V. V. Grushin, *Chem. Commun.*, 2015, **51**, 13527.
34. U. Koelle, M. H. Wang and G. Raabe, *Organometallics*, 1991, **10**, 2573.
35. S. D. Loren, B. K. Campion, R. H. Heyn, T. D. Tilley, B. E. Bursten and K. W. Luth, *J. Am. Chem. Soc.*, 1989, **111**, 4712.
36. K. Moudgil, M. A. Mann, C. Risko, L. A. Bottomley, S. R. Marder and S. Barlow, *Organometallics*, 2015, **34**, 3706.
37. S. Zhang, K. Moudgil, E. Jucov, C. Risko, T. V. Timofeeva, S. R. Marder and S. Barlow, *Inorg. Chim. Acta*, 2019, **489**, 67.
38. W. E. Britton, R. Kashyap, M. El-Hashash, M. El-Kady and M. Herberhold, *Organometallics*, 1986, **5**, 1029.
39. K.-P. Stahl, G. Boche and W. Massa, *J. Organomet. Chem.*, 1984, **277**, 113.
40. J. L. Dye, K. D. Cram, S. A. Urbin, M. Y. Redko, J. E. Jackson and M. Lefenfeld, *J. Am. Chem. Soc.*, 2005, **127**, 9338.
41. O. V. Gusev, M. G. Peterleitner, M. A. Ievlev, A. M. Kal'sin, P. V. Petrovskii, L. I. Denisovich and N. A. Ustynyuk, *J. Organomet. Chem.*, 1997, **531**, 95.
42. V. G. Andrianov, Y. T. Struchkov, V. A. Petrakova and N. A. Vol'kenau, *Koord. Khim.*, 1986, **12**, 978.
43. S. Lee, S. R. Lovelace, Debra J. Arford, S. J. Geib, S. G. Weber and N. J. Cooper, *J. Am. Chem. Soc.*, 1996, **118**, 4190.

44. M. V. Gaudet, A. W. Hanson, P. S. White and M. J. Zaworotko, *Organometallics*, 1989, **8**, 286.
45. M. Tamm, T. Bannenberg, R. Fröhlich, S. Grimme and M. Gerenkamp, *Dalton Trans.*, 2004, 482.
46. L. Shao, S. J. Geib, P. D. Badger and N. J. Cooper, *J. Am. Chem. Soc.*, 2002, **124**, 14812.
47. P. B. Hitchcock, M. F. Lappert and A. V. Protchenko, *J. Am. Chem. Soc.* , 2001, **123**, 189.
48. S. Guo, S. K. Mohapatra, A. Romanov, T. V. Timofeeva, K. I. Hardcastle, K. Yesudas, C. Risko, J.-L. Brédas, S. R. Marder and S. Barlow, *Chem. Eur. J.*, 2012, **18**, 14760.
49. B. Steinmetz and W. A. Schenk, *Organometallics*, 1999, **18**, 943.
50. Y. Zhao and D. Truhlar, *Theor. Chem. Acc.*, 2008, **120**, 215.
51. M. M. Francl, W. J. Pietro, W. J. Hehre, J. S. Binkley, M. S. Gordon, D. J. DeFrees and J. A. Pople, *J. Chem. Phys.*, 1982, **77**, 3654.
52. P. C. Hariharan and J. A. Pople, *Theor. Chim. Acta*, 1973, **28**, 213.
53. T. H. Dunning_Jr. and P. J. Hay, in *Modern Theoretical Chemistry*, ed. H. F. Schaefer III, Plenum, New York, 1977, vol. 3, pp. 1.
54. P. J. Hay and W. R. Wadt, *J. Chem. Phys.*, 1985, **82**, 299.
55. P. J. Hay and W. R. Wadt, *J. Chem. Phys.*, 1985, **82**, 270.
56. M. J. Frisch, G. W. Trucks, H. B. Schlegel, G. E. Scuseria, M. A. Robb, J. R. Cheeseman, G. Scalmani, V. Barone, B. Mennucci, G. A. Petersson, H. Nakatsuji, M. Caricato, X. Li, H. P. Hratchian, A. F. Izmaylov, J. Bloino, G. Zheng, J. L. Sonnenberg, M. Hada, M. Ehara, K. Toyota, R. Fukuda, J. Hasegawa, M. Ishida, T. Nakajima, Y. Honda, O. Kitao, H. Nakai, T. Vreven, J. A. Montgomery_Jr., J. E. Peralta, F. Ogliaro, M. Bearpark, J. J. Heyd, E. Brothers, K. N. Kudin, V. N. Staroverov, T. Keith, R. Kobayashi, J. Normand, K. Raghavachari, A. Rendell, J. C. Burant, S. S. Iyengar, J. Tomasi, M. Cossi, N. Rega, J. M. Millam, M. Klene, J. E. Knox, J. B. Cross, V. Bakken, C. Adamo, J. Jaramillo, R. Gomperts, R. E. Stratmann, O. Yazyev, A. J. Austin, R. Cammi, C. Pomelli, J. W. Ochterski, R. L. Martin, K. Morokuma, V. G. Zakrzewski, G. A. Voth, P. Salvador, J. J. Dannenberg, S. Dapprich, A. D. Daniels, O. Farkas, J. B. Foresman, J. V. Ortiz, J. Cioslowski and D. J. Fox, *Gaussian 09, Revision E.01*, Gaussian Inc., Wallingford CT, 2013.
57. S. Jhulki, H.-I. Un, Y.-F. Ding, C. Risko, S. K. Mohapatra, J. Pei, S. Barlow and S. R. Marder, *Chem*, 2021, **7**, 1050.
58. F. Barriere, N. Camire, W. E. Geiger, U. T. Mueller-Westerhoff and R. Sanders, *J. Am. Chem. Soc.*, 2002, **124**, 7262.